Electronic Supplementary Material (ESI) for Journal of Materials Chemistry A.

Extended Data: Safety issues caused by internal short circuits in lithium-ion batteries

1 Introduction

Abusive conditions, such as mechanical loading, over-heat and over-charge pose a threatening situation for the potential hazardous scenarios for LIBs. Those negative effects may directly trigger the ISC for the cell, followed by a sequence of physical, chemical and electrical changes for the materials (Fig. S1). With the onset of ISC, produced heat by ohm law raises the temperature. SEI (Solid-Electrolyte-Interphase) may resolve above 90℃, followed by the inserted lithium in anode reaction with electrolyte. Separator usually starts to melt from 130℃. Decomposition of electrolyte initiates at around 200℃ and binder for the active particles on electrodes involves into reaction above 260℃. Above 660℃, Al collector starts melting. Whether there is a safety boundary/vicinity if the ISC is triggered and how many typical types of electrochemical behavior of cells after ISC still remain unknown.

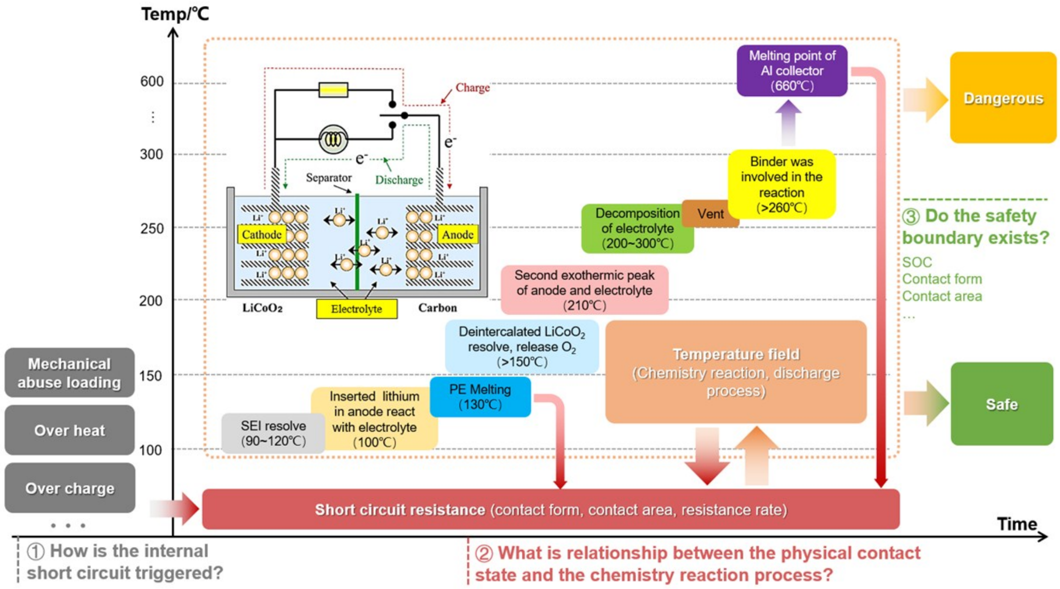

Fig. S1. Physical ang chemical process of internal short-circuit of lithium battery.

2 Experimental

2.1. Penetration test.

Four repeated tests were conducted to make sure the repeatability and confidence of the indentation tests to trigger the ISC (Fig. S2). The highly consistent results again directly proves the credibility of such methodology.

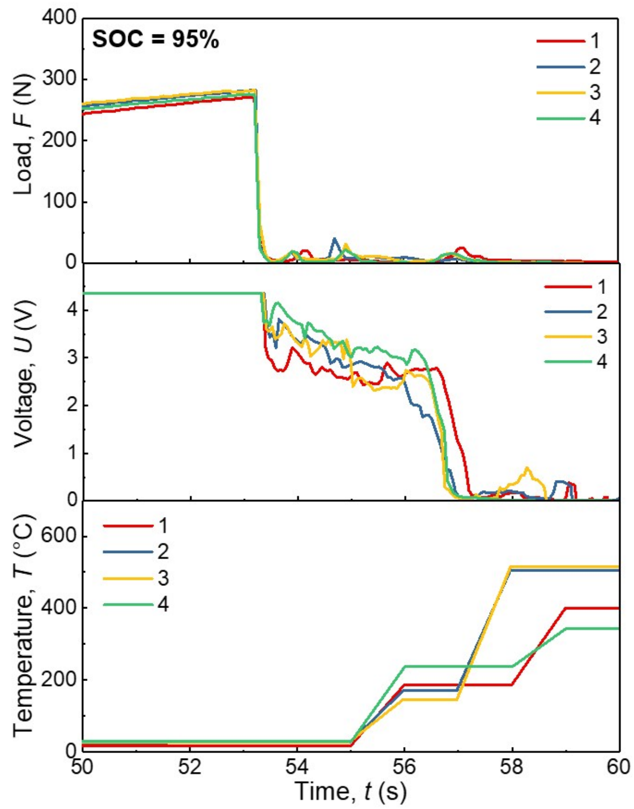

Fig. S2. Repeated experiment results for High SOC (95%) batteries.

Table S1. Specifications of equipment for experiments of Cases 1 and 2.

Equipment	Type	Range	Frequency	Precision	Resolution ratio
Universal material testing machine	INSTRON 2345	±5 kN	10 Hz	±(5%×RD + 0.005%×10 kN)	50 N
Digital voltmeter	Agilent 34410A	0~10 V	20 Hz	±(0.0015×RD +0.0004ΔT)	0.01 mV
Multi-channel temperature sensors	ANBAI AT4508	200 ℃~ 1300 ℃	1 Hz	±0.2 ℃	0.1 ℃
Battery performance	BK6808AR	0~5 V 0~5 A	1 Hz	±(0.05%RD +0.05%FS)	1 mV 1 mA

testing machine

2. 2. Contact resistance measurement experiment.

The relationship between contact resistance and contact stress was shown in Fig.S3.

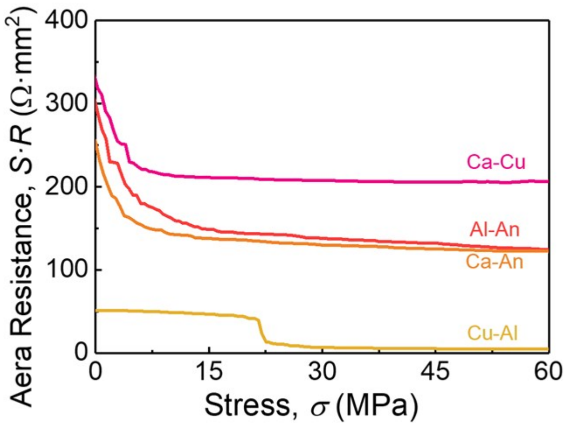

Fig. S3. contact stress -resistance curves.

3. Modeling and calibrating FE of LIB

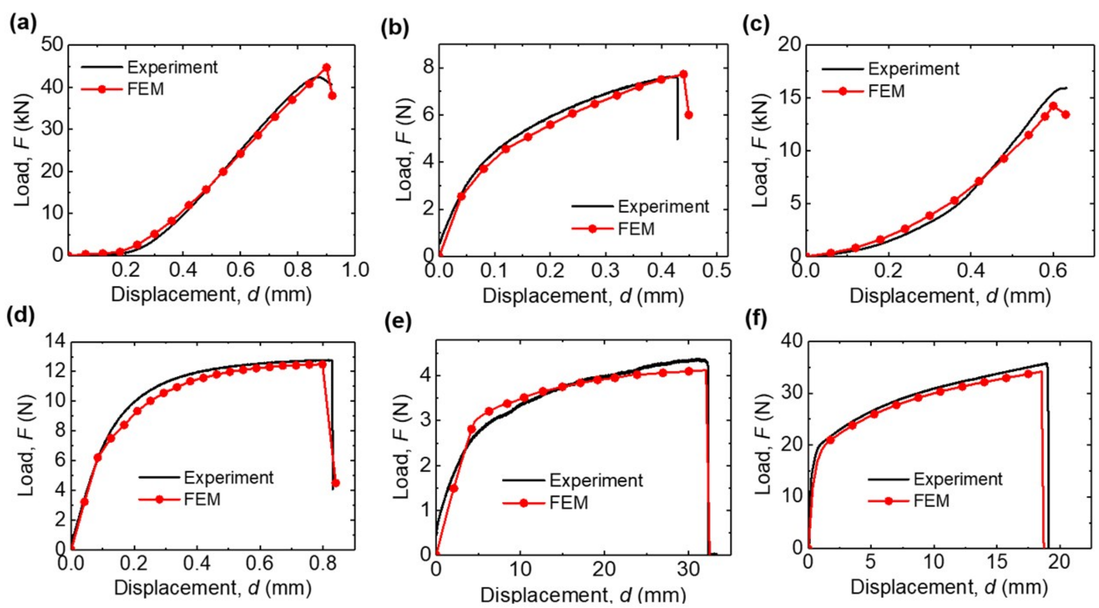

Fig. S4. The comparison of experiment and simulation for (**a**) cathode compression, (**b**) cathode tension, (**c**) anode compression, (**d**) anode tension, (**e**) separator tension, (**f**) cover shell tension.

Table S2 Parameters and setups for mechanical model of LIB

	Material	Thickness (um)	Mechanical model	Young's Modulus (MPa)	Yield stress (MPa)	Hardening curve (MPa)	Element type
Cover	Al plastic film	76	Elastic-plastic	1221	27.4	$\sigma_p^{\mathrm{cov}} = \sigma_0^{\mathrm{cov}} + 55.6\varepsilon_p^{\mathrm{cov}\,0.32}$	S4R
Separator	PP	8	Elastic-plastic	572	80.69	$\sigma_p^{sep} = \sigma_0^{sep} + 280\varepsilon_p^{sep\,1.118}$	C3D8R
Current collector (Anode)	Cu	6	Elastic-plastic	74400	200.3	$\sigma_p^{ncc} = \sigma_0^{ncc} + 1286\varepsilon_p^{ncc\,0.059}$	S4R
Current collector (cathode)	Al	10	Elastic-plastic	35000	60.02	$\sigma_p^{pcc} = \sigma_0^{pcc} + 824.3\varepsilon_p^{pcc\,0.46}$	S4R
Anode	LiC_x	104	Crushable foam	1200	0.1	$\sigma_p^{neg} = \sigma_0^{neg} + 1419.2\varepsilon_p^{pcc\,2.32}$	C3D8R
Cathode	$LiCoO_2$	127	Crushable foam	500	0.1	$\sigma_p^{pos} = \sigma_0^{pos} + 3086.9\varepsilon_p^{pos\,2.24}$	C3D8R

4. Multi-physics method of LIB

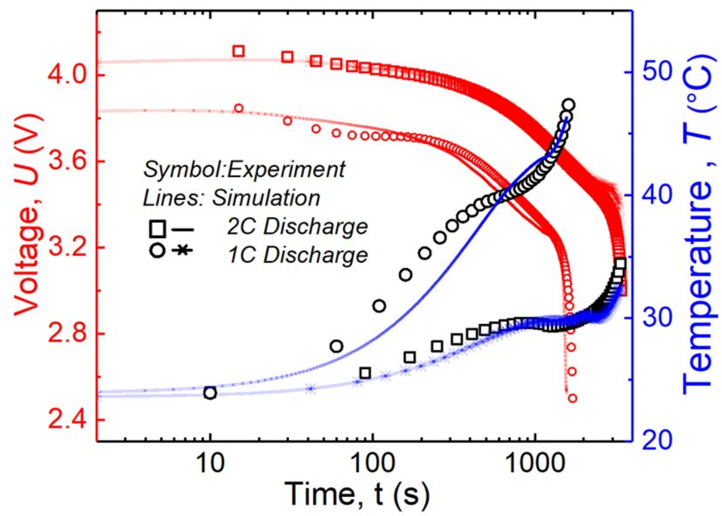

Fig. S3. Comparison results for experiment and simulation for LIB during discharge.

Table S3 Governing equations of all sub-models

Model	Function name	Function
	Cell potential	$E_v^{cell} = \phi^{s,pos} - \phi^{s,neg} = E_v^{pos} - E_v^{neg} - \Delta\phi^{l}$
	Cell current	$i^{cell} = \frac{\Delta\phi_l}{R_r^{sol}}$, $I^{cell} = A^{sep} i^{cell}$, $A^{sep} = \frac{\varepsilon^{sep} V^{cell}}{L^{sep}}$
	Charge balance	$\pm i^{cell} \frac{A^{sep}}{V^{cell}} = \varepsilon^{s} \left(\sum_m A_{v,m} i_{loc,m} + A_{v,dl} i_{dl} \right)$
	Diffusion equation	$r^2 \frac{\partial c^s}{\partial t} + \frac{}{\partial r} D^s \frac{\partial c^s}{\partial r} = 0$, $-D^s \frac{\partial c^s}{\partial r} = -R_\theta^s \Big\|_{r=r_p}$, $\frac{\partial c^s}{\partial r} = 0 \Big\|_{r=0}$ $R_\theta^s = -\sum_m \frac{v_{\theta,m}^s}{n_m F} \frac{A_m^v}{N_{shape} \varepsilon^s / r_p}$
Battery model[1-3]	Battery heat	$Q^s = \varepsilon^{s} \sum_m A_{v,m} i_{loc,m} (E_p - E_{p,m}^{eq} + T \frac{\partial E_{p,m}^{eq}}{\partial T})$, $Q^{sol} = \frac{\Delta\phi^l i^{cell} A^{sep}}{V^{cell}}$ $Q_{ba} = Q^{neg} + Q^{pos} + Q^{sol}$
	Electrode kinetics expression	$i_0 = F (k^{pos})^{\alpha^{neg}} (k^{neg})^{\alpha^{pos}} (c_{\max}^s - c^s)^{\alpha^{neg}} (c^s)^{\alpha^{pos}} (\frac{c^l}{c_{ref}^l})$ $i_{loc} = i_0 \left(\exp\left(\frac{\alpha^{neg} F \eta}{R_g T} \right) - \exp\left(\frac{-\alpha^{pos} F \eta}{R_g T} \right) \right)$
Thermal runaway model[4, 5]	SEI decomposition	$Q^{sei} = H^{sei} W_c A^{sei} \exp[\frac{-E_a^{sei}}{R_g T}] c_{sei}$, $\frac{dc^{sei}}{dt} = -A^{sei} \exp[\frac{-E_a^{sei}}{R_g T}] c_{sei}$

	anode–electrolyte reaction	$\frac{dc_a}{dt}=-A^{a-e}\exp[\frac{-z}{z_0}]\exp[\frac{-E_a^{a-e}}{R_gT}]c_a$ $Q^{a-e}=H^{a-e}W_cA^{a-e}\exp[\frac{-z}{z_0}]\exp[\frac{-E_a^{a-e}}{R_gT}]c_a$ $\frac{dz}{dt}=-A^{a-e}\exp[\frac{-z}{z_0}]\exp[\frac{-E_a^{a-e}}{R_gT}]c_a$
	cathode–electrolyte reaction	$Q^{c-e}=H^{c-e}W_pA^{c-e}\alpha^{c-e}(1-\alpha^{c-e})\exp[\frac{-E_a^{c-e}}{R_gT}]$ $\frac{d\alpha^{c-e}}{dt}=A^{c-e}\alpha^{c-e}(1-\alpha^{c-e})\exp[\frac{-E_a^{c-e}}{R_gT}]$
	electrolyte decomposition reaction	$Q^e=H^eW_eA^e\exp[\frac{-E_a^e}{R_gT}]c_e$ $\frac{dc_e}{dt}=-A^e\exp[\frac{-E_a^e}{R_gT}]c_e$
	thermal runaway heat	$Q_{tr}=Q^{sei}+Q^{a-e}+Q^{c-e}+Q^e$
Mechanical model[6]	Governing equation	$\rho\frac{\partial^2\boldsymbol{u}}{\partial t^2}=\nabla_X(F_LS)+\mathrm{F}_V$
	Governing equation	$\vec{j}=\kappa^{St}\vec{\nabla}\phi$, $Q_{st}=\frac{\vec{j}\cdot\vec{j}}{\kappa^{St}}$
Short circuit model[6, 7]	Melting of separator and current collector	$\frac{dc_{sep}}{dt}=-A^{sep}\exp[\frac{-E_a^{sep}}{R_gT}]c_{sep}$ $\frac{dc_{cc}}{dt}=-A^{cc}\exp[\frac{-E_a^{cc}}{R_gT}]c_{cc}$
	Electric conductivity	$\kappa^{cc}=\kappa_0^{cc}c_{cc}+\kappa_e^{cc}$, $\kappa^{sep}=\kappa_e^{sep}*(1-c_{sep})+\kappa_0^{sep}$
Thermal model[4, 8]	Governing equation	$\rho C_p(\frac{\partial T}{\partial t}+\boldsymbol{u}\nabla T)+\nabla\boldsymbol{q}=Q$, $\boldsymbol{q}=-k\nabla T$,

	$Q = Q_{ba} + Q_{st} + Q_{tr}$
Boundary condition	$-\boldsymbol{n} \cdot \boldsymbol{q}_{fl} = h^{cell}(T_{amb} - T)$,
	$-\boldsymbol{n} \cdot \boldsymbol{q}_{df} = \varepsilon_{Df} \sigma_{B-D}(T_{amb}^4 - T^4)$

Nomenclature

A: Arrhenius constants (1)

A_v: active specific surface area

c: concentration ($\mathrm{mol/m^3}$)

c_{sei}: dimensionless amount of lithium-containing metastable species in the solid electrolyte interphase (SEI) (1)

c_{sei0}: initial value of the dimensionless amount of lithium-containing metastable species in the SEI (1)

c_a: dimensionless amount of lithium intercalated within carbon (1)

c_{a0}: initial value of the dimensionless amount of lithium intercalated within carbon (1)

c_{cc}: dimensionless amount of solid phase of current collector (1)

c_e: dimensionless concentration of electrolytes (1)

c_{e0}: initial value of the dimensionless concentration of electrolytes (1)

c_{sep}: dimensionless amount of solid phase of separator (1)

C_p: heat capacity ($\mathrm{J/(kg \cdot K)}$)

D: diffusion coefficient ($\mathrm{m^2/s}$)

E: Young's modulus (MPa)

E_p : Potential (V)

E_a : experimental activation energy (J/mol)

F : Faraday's constant ($9.64853\times10^4\,\mathrm{C/mol}$)

H : heat transfer coefficients(J/g)

h : heat transfer coefficient ($\mathrm{W/(m^2\cdot K)}$)

I : current (A)

i : current density ($\mathrm{A/m^2}$)

i_0: exchange current density ($\mathrm{A/m^2}$)

i_{loc}: local intercalation current density ($\mathrm{A/m^2}$)

i_{dl}: double layer current density ($\mathrm{A/m^2}$)

k: thermal conductivity ($\mathrm{W/(m\cdot K)}$)

SOC : state of charge value

t : time (s)

t_+: transfer data

W_c : volume-specific carbon content ($\mathrm{g/m^3}$)

W_p : volume-specific positive active content ($\mathrm{g/m^3}$)

W_e volume-specific electrolyte content in the jellyroll ($\mathrm{g/m^3}$)

z : dimensionless measure of the SEI layer thickness (1)

z_0 : reference dimensionless measure of the SEI layer thickness (1)

Q : heat sources ($\mathrm{W/m^3}$)

Q_{ba} : heat for battery model ($\mathrm{W/m^3}$)

Q_{st} : heat from the short-circuit model ($\mathrm{W/m^3}$)

Q_{tr} : heat from the thermal runaway model ($\mathrm{W/m^3}$)

$\boldsymbol{q}$: heat flux ($\mathrm{W/m^2}$)

$\boldsymbol{q}_{fl}$: heat flux by conduction ($\mathrm{W/m^2}$)

$\boldsymbol{q}_{df}$: heat flux by radiation ($\mathrm{W/m^2}$)

R : radius (mm)

R_g : gas constant

R_r : resistance (Ω)

R_θ : molar flux of lithium at the particle surface

t_+ : transfer data

T: temperature (K)

T_{abm}: Ambient temperature

α : conversion degree (1)

α_0 : initial value of the conversion degree (1)

α_m : ratio of tension and compression (1)

ρ : density ($\mathrm{kg/m^3}$)

σ_{B-D} : Stefan–Boltzmann constant ($5.67\times10^{-8}\ \mathrm{W/(m^2\times K^4)}$)

σ_0 : yield stress (MPa)

ε_p : plastic strain (1)

δ : thickness (mm)

ò: volume fraction

ε : strain (1)

ε_{Df} : surface emissivity (1)

κ : electrical conductivity (S/m)

κ_0 : initial electrical conductivity (S/m)

κ_e : electrical conductivity after melting (S/m)

ν : Poisson's ratio

v_θ : Stoichiometric coefficient of the intercalating species

ϕ : potential (V)

$1+\frac{\mathrm{d}\ln f}{\mathrm{d}\ln c^l}$: molar activity coefficient

Subscripts

eff: modified

Superscripts

a-e: anode–electrolyte reaction

c-e: cathode–electrolyte reaction

cell: the cell (LIB)

cov: cover shell

e: electrolyte decomposition

eq: equilibrium

D: diffusion

LB: lithium-ion battery

l: liquid (electrolyte)

ncc: negative collector

neg: negative electrode

pcc: positive collector

pos: positive electrode

sei: SEI decomposition reaction

s: solid (electrode)

sep: separator

sol: solution

St: short-circuit model

Supplementary Videos

Video 1. Experiment process of triggered internal short-circuit and thermal runway of lithium-ion pouch cell at 95% SOC.
Video 2. Multiphysics sub-model simulation process of lithium-ion pouch cell with 95% SOC by mechanical indentation.
Video 3. Multiphysics sub-model simulation process of lithium-ion pouch cell with 60% SOC by mechanical indentation.

References

1. C. M. Doyle, T. F. Fuller and J. S. Newman, *Journal of The Electrochemical Society*, 1993, **140**, 1526–1533.
2. T. F. Fuller, M. Doyle and J. Newman, *Journal of the Electrochemical Society*, 1994, **141**, 1-10.
3. C. M. Doyle, Doctor, University of California, 1995.
4. T. D. Hatchard, D. D. Macneil, A. Basu and J. R. Dahn, *Journal of the Electrochemical Society*, 2001, **148**, A755-A761.
5. G. H. Kim, A. Pesaran and R. Spotnitz, *J. Power Sources*, 2007, **170**, 476-489.
6. B. Liu, H. Zhao, H. Yu, J. Li and J. Xu, *Electrochimica Acta*, 2017, DOI: https://doi.org/10.1016/j.electacta.2017.10.045.
7. B. Liu, S. Yin and J. Xu, *Applied Energy*, 2016, **183**, 278-289.
8. K.-C. Chiu, C.-H. Lin, S.-F. Yeh, Y.-H. Lin and K.-C. Chen, *J. Power Sources*, 2014, **251**, 254-263.